PHYSICAL REVIEW B **93**, 241304(R) (2016)

Quantum capacitance of an HgTe quantum well as an indicator of the topological phase

T. Kernreiter, M. Governale, and U. Zülicke
School of Chemical and Physical Sciences and MacDiarmid Institute for Advanced Materials and Nanotechnology, Victoria University of Wellington, P.O. Box 600, Wellington 6140, New Zealand

(Received 24 March 2016; revised manuscript received 30 May 2016; published 15 June 2016)

Varying the quantum-well width in an HgTe/CdTe heterostructure allows for realizing normal and inverted semiconducting band structures, making it a prototypical system to study two-dimensional (2D) topological-insulator behavior. We have calculated the zero-temperature thermodynamic density of states D_T for the electron-doped situation in both regimes, treating interactions within the Hartree-Fock approximation. A distinctively different behavior for the density dependence of D_T is revealed in the inverted and normal cases, making it possible to detect the system's topological phase through measurement of macroscopic observables, such as the quantum capacitance or electronic compressibility. Our results establish the 2D electron system in HgTe quantum wells as unique in terms of its collective electronic properties.

DOI: 10.1103/PhysRevB.93.241304

Introduction. Capacitance measurements are a premier tool to elucidate the electronic properties of two-dimensional (2D) electron systems [1–14]. They fundamentally probe the thermodynamic density of states,

$$D_T = \frac{\partial n}{\partial \mu}, \tag{1}$$

where n and μ denote the 2D system's electronic sheet density and chemical potential, respectively. More specifically, D_T is related to the quantum capacitance per unit area C_q and the electronic compressibility K via

$$C_q = e^2 D_T, \tag{2a}$$

$$K = \frac{D_T}{n^2}. \tag{2b}$$

The intriguing interplay between single-particle and Coulomb-interaction contributions to D_T has been intensely studied theoretically, both for conventional 2D electron systems realized in heterostructures [15–18] and for few-layer graphene [18–22]. In particular, the tendency towards negative electronic compressibility in the low-density limit [23] has attracted a lot of attention [3–9].

Here we show how the thermodynamic density of states of electrons in an HgTe quantum well exhibits behavior different from any of the previously studied 2D electron systems, essentially because of the anomalous properties of an interaction-related interband contribution relevant for narrow-gap systems. Our work provides new insight complementing the observation of unusual electric-transport properties in this system [24–27] that relate to the existence of an unconventional inverted 2D electronic band structure when the quantum-well width d is larger than a critical value $d_c \approx 6.3$ nm [28–31]. The deeper understanding derived from our results also enables novel characterization of topological phases [32] in other 2D [33,34] and bulk [32,35] materials and extends the general knowledge about unusual collective properties of topological and Dirac-semi-metal systems [36–38].

We calculate the thermodynamic density of states for electrons in HgTe quantum wells, taking Coulomb interactions into account within the Hartree-Fock approximation. To be specific, we focus on two experimentally feasible situations with quantum-well widths $d = 5$ and 7 nm, respectively, and present predictions for D_T as a function of the 2D-system's Fermi wave vector. In our calculations, crucial effects arising from the finite width of electronic bound states in the HgTe/CdTe heterostructure are included. Quite generally, we find that interaction contributions significantly affect D_T and, thus, observables, such as the quantum capacitance and the electronic compressibility. See Fig. 1 for a pertinent example. More specifically, it turns out that the interband exchange correction depends strongly on the quantum-well width and changes its sign for a value close to d_c. We elucidate the underlying mechanisms, such as the interplay of band-structure parameters that lead to this interesting behavior.

Model and Formalism. The theoretical framework for our calculation of many-particle effects for electrons in an HgTe quantum well is based on the Bernevig-Hughes-Zhang (BHZ) Hamiltonian [28]. The latter adequately describes the relevant single-particle states in the low-energy band structure using basis functions $|E_1\pm\rangle$, which are superpositions of conduction-electron and light-hole (LH) states, and the heavy-hole (HH) states $|H_1\pm\rangle$. Within the representation defined by the basis-state vector $(|E_1+\rangle,|H_1+\rangle,|E_1-\rangle,|H_1-\rangle)$, the BHZ Hamiltonian is block diagonal and given by

$$\mathcal{H}_0 = \begin{pmatrix} \mathcal{H}^{(+)} & 0 \\ 0 & \mathcal{H}^{(-)} \end{pmatrix}, \tag{3}$$

with $\mathcal{H}^{(s)} = h^{(s)}_\mu \sigma^\mu$, $h^{(s)} = (C - Dk^2, sAk_x, -Ak_y, M - Bk^2)$, and $\sigma^\mu = (\mathbb{1},\sigma_x,\sigma_y,\sigma_z)$ where σ_j are the Pauli matrices. The quantum number $s = \pm 1$ distinguishes spin-1/2 projections parallel to the quantum-well growth direction, and the effective band-structure parameters A, B, C, D, M are functions of the quantum-well width d [39]. For simplicity, we set the irrelevant overall energy shift C to zero. The sign of the gap parameter M distinguishes the ordinary and inverted-band situations: Using the convention $B < 0$, the system is in the topological (normal) regime when $M < 0$ ($M > 0$).

The energy eigenvalues of the BHZ Hamiltonian (3) are given by [28]

$$E^{(s)}_{\mathbf{k}\alpha} \equiv E^{(s)}_{k\alpha} = -Dk^2 + \alpha\sqrt{(M - Bk^2)^2 + A^2k^2}, \tag{4}$$

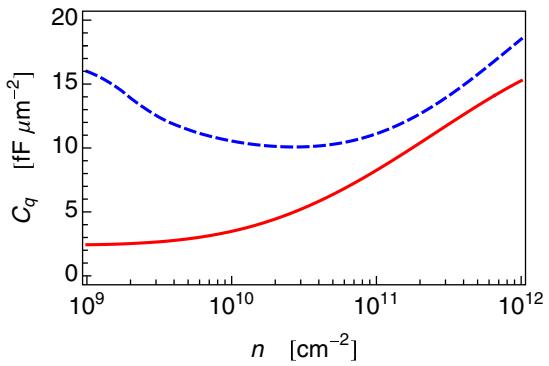

FIG. 1. Density dependence of the quantum capacitance per unit area for electrons in an HgTe quantum well. The red solid (blue dashed) curve is obtained for a quantum-well width $d =$ 7 nm (5 nm) corresponding to the topological (normal) situation. Clearly distinguishable opposite trends emerge in the low-density regime.

where $\alpha = \pm 1$ distinguishes conduction and valence bands, both of which are doubly degenerate in s. Due to the inherent axial symmetry of the BHZ model, the eigenvectors of the two 2×2 matrices $\mathcal{H}^{(s)}$ in Eq. (3) can be expressed as $a^{(s)}_{\mathbf{k}\alpha} = U^{(s)}_{\phi_\mathbf{k}} a^{(s)}_{k\alpha}$ in terms of the polar coordinates $(k,\phi_\mathbf{k})$ for wave-vector $\mathbf{k}$ with

$$a^{(s)}_{k\alpha} = \frac{1}{\sqrt{2}} \begin{pmatrix} \alpha\left[1 - \frac{\alpha(Bk^2-M)}{\sqrt{A^2k^2+(Bk^2-M)^2}}\right]^{1/2} \\ s\left[1 + \frac{\alpha(Bk^2-M)}{\sqrt{A^2k^2+(Bk^2-M)^2}}\right]^{1/2} \end{pmatrix}, \tag{5}$$

and $U^{(s)}_{\phi_\mathbf{k}} = \mathrm{diag}(e^{is\phi_\mathbf{k}/2}, e^{-is\phi_\mathbf{k}/2})$.

Quantum many-body effects. The single-particle band dispersions given in Eq. (4) are renormalized by interaction effects. Assuming that the electrostatic (Hartree) terms are compensated by the influence of a neutralizing background charge density, we focus here on the exchange (Fock) contributions. The fundamental quasi-2D character of the charge carriers is accounted for by retaining the full z dependence of quantum-well bound states through the basis functions $|E_1+\rangle, |H_1+\rangle, |E_1-\rangle, |H_1-\rangle$ for the BHZ Hamiltonian. The Fock self-energy of conduction-band electrons can then be written as

$$\Sigma^{(s)}_{k\pm} = -2\pi C \int \frac{d^2k'}{(2\pi)^2} n_\mathrm{F}\big(E^{(s)}_{\mathbf{k}'\pm}\big) \int dz \int dz' \frac{e^{-|\mathbf{k}-\mathbf{k}'||z-z'|}}{|\mathbf{k}-\mathbf{k}'|} \times \big[\psi^{(s)}_{\mathbf{k}'\pm}(z)^\dagger \psi^{(s)}_{\mathbf{k}+}(z)\big]\big[\psi^{(s)}_{\mathbf{k}+}(z')^\dagger \psi^{(s)}_{\mathbf{k}'\pm}(z')\big], \tag{6}$$

where $C = e^2/(4\pi\epsilon\epsilon_0)$ measures the Coulomb-interaction strength, $n_\mathrm{F}(E)$ is the Fermi function, and the $\psi^{(s)}_{\mathbf{k}\alpha}(z)$ are six-dimensional spinor wave functions comprising the bands with Γ_6 and Γ_8 symmetry closest to the bulk-material's fundamental gap [40]. Intra- (inter-) band contributions to the Fock self-energy are labeled by the subscripts $+$ $(-)$. Note that terms with $s \neq s'$ vanish for the block-diagonal BHZ model given above because of the orthogonality of the associated basis states. However, such contributions do arise when spin-orbit-coupling effects are included. Effects of the latter will be discussed briefly at the end of this Rapid Communication.

In the zero-temperature limit, which we consider in the following, the Fermi functions in Eq. (6) reduce to $n_\mathrm{F}(E^{(s)}_{\mathbf{k}-}) = 1$ for the fully occupied valence band and $n_\mathrm{F}(E^{(s)}_{\mathbf{k}+}) = \Theta(k_\mathrm{F} - |\mathbf{k}|)$, where k_F is the modulus of the Fermi wave vector for electrons in the conduction band and $\Theta(\cdot)$ denotes the Heaviside step function. To take into account both the in-plane dynamics described by the BHZ Hamiltonian as well as the nontrivial spinor structure of the BHZ-model basis states, we employ sub-band $\mathbf{k}\cdot\mathbf{p}$ theory [41,42] to write the spinor wave functions $\psi^{(s)}_{\mathbf{k}\alpha}(z)$ as superpositions,

$$\psi^{(s)}_{\mathbf{k}\alpha}(z) = \sum_{i=1}^{2} \big(U^{(s)}_{\phi_\mathbf{k}}\big)_{ii} a^{(s)}_{k\alpha,i} \psi^{(s)}_{0i}(z), \tag{7}$$

where the coefficients $a^{(s)}_{k\alpha,i}$ are the components of the corresponding eigenvectors Eq. (5) of the BHZ Hamiltonian. The six-dimensional spinors $\psi^{(s)}_{0i}(z)$ are the BHZ-model basis-state spinors for vanishing in-plane wave vector, which are determined by the solutions to a confined-particle problem for the HgTe/CdTe quantum-well heterostructure. Their explicit expressions have been given in the Supplemental Material of Ref. [28] where for instance $\psi^{(+)}_{01}(z)^T = [f_1(z),0,0,f_4(z),0,0]$ and $\psi^{(+)}_{02}(z)^T = [0,0,f_3(z),0,0,0]$ which are normalized, i.e., $\int dz |\psi^{(s)}_{0i}(z)|^2 = 1$, $\forall\, i,s$. As a result, we obtain for the intra- and interband contributions to the Fock self-energy,

$$\Sigma^{(s)}_{k\pm} = \frac{-C}{\pi} \int_0^\pi d\phi \int_0^{k_\pm} dk' k' \int dz \int dz' \frac{e^{-r(k,k',\phi)|z-z'|}}{r(k,k',\phi)} \times \sum_{i,j} \mathcal{F}_{ij}(\phi) a^{(s)}_{k'\pm,i} a^{(s)}_{k'\pm,j} a^{(s)}_{k+,i} a^{(s)}_{k+,j} \big|\psi^{(s)}_{0i}(z)\big|^2 \big|\psi^{(s)}_{0j}(z')\big|^2, \tag{8}$$

where the integration limits are $k_+ = k_\mathrm{F}$ (intraband) and $k_- = k_\mathrm{c}$ (interband) with k_c being an ultraviolet cutoff. In Eq. (8), $r(k,k',\phi) = \sqrt{k^2 + k'^2 - 2kk'\cos\phi}$ and $\mathcal{F}_{ij}(\phi) = \sqrt{1-(1-\delta_{ij})\sin^2\phi}$, with $\phi \equiv \phi_\mathbf{k} - \phi_{\mathbf{k}'}$ and δ_{ij} being the Kronecker symbol. The interband contribution depends logarithmically on k_c, which is typically chosen to be on the order of the inverse lattice constant [19,20]. Finally, with the chemical potential given in terms of k_F as $\mu = E^{(s)}_{k_\mathrm{F}+} + \Sigma^{(s)}_{k_\mathrm{F}+} + \Sigma^{(s)}_{k_\mathrm{F}-}$ and using the relation $n = k_\mathrm{F}^2/(2\pi)$, the expression (1) for the thermodynamic density of states can be rewritten as $D_\mathrm{T} = \left(\frac{\pi}{k_\mathrm{F}} \frac{\partial\mu}{\partial k_\mathrm{F}}\right)^{-1}$. Measuring wave vectors and energies in terms of the BHZ-model scales $q_0 \equiv A/|B|$ and $E_0 \equiv Aq_0$, the natural unit for D_T^{-1} is $|B|$. The fine-structure constant that appears in the exchange-energy contributions to μ is given by $\alpha_\mathrm{qw} \equiv e^2/(4\pi\epsilon\epsilon_0 A) \approx 0.19$ when using $\epsilon = 20.8$ as the dielectric constant of HgTe.

Numerical results for D_T. We now present results obtained for the thermodynamic density of states in normal and topological HgTe quantum wells. Following the usual convention, $D_\mathrm{T}^{-1} \equiv \partial\mu/\partial n$ is shown as a function of the Fermi wave vector. We first consider an HgTe quantum well with width $d = 5$ nm, which is in the the normal (noninverted band-structure) regime. The associated BHZ parameters are given in Table I and correspond to an actual experimental realization [39]. For the large-momentum cutoff of the interband contribution,

TABLE I. Parameters of the BHZ model applicable for two experimental realizations of HgTe quantum wells [39] having widths of $d = 5$ and 7 nm, respectively.

	$d = 5$ nm	$d = 7$ nm
A (eV nm)	0.365	0.340
B (eV nm^2)	−0.50	−0.50
D (eV nm^2)	−0.50	−0.87
M (meV)	24.0	−8.5

we choose $k_c = a_0^{-1}$ with $a_0 = 0.646$ nm being the HgTe bulk-material lattice constant. We show the result obtained for D_T^{-1} in Fig. 2, also making explicit the various contributions to D_T^{-1}. The purely kinetic (i.e., noninteracting) part is given by a constant in the low-density regime,

$$\left.\frac{\partial E^{(s)}_{k_F\alpha}}{\partial n}\right|_{k_F=0} = 2\pi\left[\alpha\left(\frac{A^2}{2|M|} + |B|\mathrm{sgn}(M)\right) - D\right], \quad (9)$$

which has the form expected for an ordinary 2D electron system [43]. However, it exhibits a weak dependence on k_F at larger carrier densities due to the HH-LH mixing of quantum-well bound states having a finite in-plane wave vector. The intraband interaction (Fock) renormalization term is always negative and therefore reduces D_T^{-1}, thus leading to an enhancement of the electronic compressibility. At low-enough densities, the intraband contribution drives D_T^{-1} to negative values. Such a behavior is also reminiscent of that of an ordinary 2D electron system [44]. In the normal regime (except very close to the critical well width d_c), the interband exchange contribution is also negative and thus reduces D_T^{-1} further. As a result, the crossover from positive to negative values of D_T^{-1} is shifted to higher densities. This behavior has to be contrasted with that exhibited by single-layer graphene where the exchange renormalization of D_T^{-1} is positive [19,20]. Overall, from the results shown in Fig. 2, we see that the exchange contributions strongly influence the electronic compressibility.

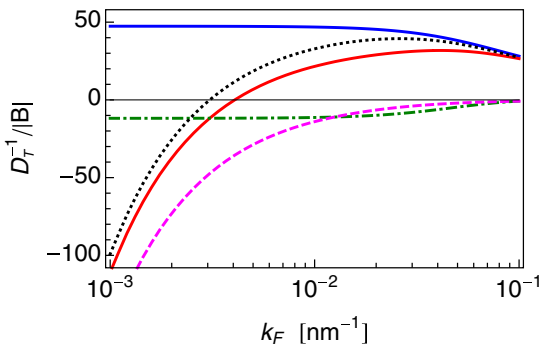

FIG. 2. Inverse thermodynamic density of states $D_T^{-1} \equiv \partial\mu/\partial n$ of an HgTe quantum well in the normal regime (well width of $d = 5$ nm). The red (blue) solid curve shows the result with (without) interactions. The magenta dashed (green dot-dashed) curve is the intraband (interband) exchange contribution only. The black dotted curve is the sum of the noninteracting and intraband exchange contributions.

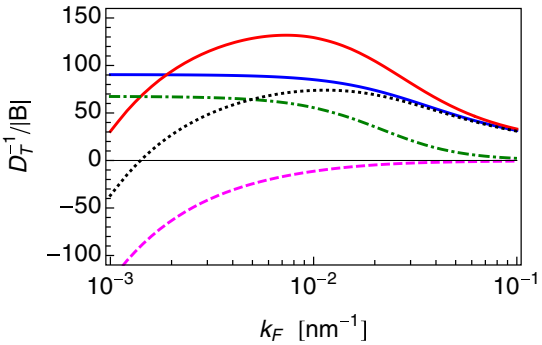

FIG. 3. Inverse thermodynamic density of states $D_T^{-1} \equiv \partial\mu/\partial n$ of an HgTe quantum well in the inverted regime (well width of $d = 7$ nm). The red (blue) solid curve shows the result with (without) interactions. The magenta dashed (green dot-dashed) curve is the intraband (interband) exchange contribution only. The black dotted curve is the sum of the noninteracting and intraband exchange contributions. Notice the positive sign of the interband exchange contribution (green dot-dashed curve), which shifts the crossover to negative compressibility to very low carrier densities.

We now consider the inverted regime of an HgTe quantum well, which is realized for a well width of $d > d_c \approx 6.3$ nm. Taking the BHZ parameters of a feasible experimental situation corresponding to a well width of $d = 7$ nm (see Table I), we again calculate the quantity D_T^{-1}. The result is shown in Fig. 3. The most salient feature is that the interband exchange contribution is now *positive*, as in single-layer graphene [19,20], and considerably larger in magnitude as compared to the situation in the normal regime. In contrast, the intraband exchange term is of similar magnitude and has the same sign as in the normal case. The kinetic (noninteracting) contribution is much larger as compared to the $d = 5$-nm case, which is mainly due to the smaller band gap in the present case—this can be inferred from Eq. (9). We see that the electronic compressibility is reduced by up to 35% due to exchange effects as compared with the noninteracting case. This trend is changed only at very low densities where the (negative) intraband contribution becomes dominant.

The striking difference observed between the interband interaction-renormalization contributions in the topological and the normal regimes invites more detailed scrutiny. Figure 4 illustrates the variation of intraband and interband exchange terms as a function of the quantum-well width [45] for a fixed carrier density of $n = 10^{10}$ cm^{-2}. The intraband contribution is always negative and rather insensitive to a variation of d. The interband contribution, however, depends strongly on the quantum-well width and changes its sign in the vicinity of the critical value of $d_c \approx 6.3$ nm. Also around d_c, due to the vanishing band gap, we can anticipate the onset of a divergence in the interband contribution for $k_F \to 0$. Figure S1 in the Supplemental Material [46] shows this even more clearly. We can attribute the sign change in the interband exchange contribution to D_T^{-1} to a complex interplay of band-mixing effects (due to the terms proportional to A in the BHZ Hamiltonian) and the change in the band characters when crossing over from $M > 0$ to $M < 0$. To be more specific, we find that the heavy-hole term ($i = j = 2$) in Eq. (8) gives

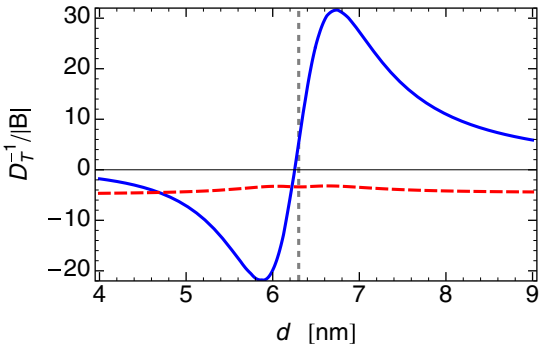

FIG. 4. Intraband (dashed red curve) and interband (solid blue curve) exchange contributions to the inverse thermodynamic density of states D_{T}^{-1} as a function of the HgTe quantum-well width d for a carrier sheet density of $n = 10^{10}$ cm^{-2}. The dashed vertical line indicates the value of the critical well width of $d_{\mathrm{c}} = 6.3$ nm.

generally (especially for low densities) the largest contribution to $\Sigma^{(s)}_{k_{\mathrm{F}}-}$ (as well as to $\partial\Sigma^{(s)}_{k_{\mathrm{F}}-}/\partial n$), where for $M > 0$ ($M < 0$) it is a monotonically decreasing (increasing) function of k_{F}.

Effect of spin-orbit coupling. We have extended our calculation of the thermodynamic density of states to the situation with bulk-inversion asymmetry and structural-inversion asymmetry spin-orbit coupling [29,47] and find that, only for the largest expected magnitudes of the bulk-inversion-asymmetry energy scale of a few meV, results change quantitatively by up to 10%. However, our findings suggest that spin-orbit coupling affects the electronic compressibility of electrons in HgTe quantum wells typically only at the percent level. See the Supplemental Material for more details [46].

Conclusions. We have presented results for the thermodynamic density of states for electrons in HgTe quantum wells in experimentally feasible situations. Interaction effects have been included within the Hartree-Fock approximation. We have also taken into account the finite width of the HgTe/CdTe quantum-well heterostructure, which is necessary to account for the attenuated Coulomb repulsion in the transverse direction. Markedly different behavior is exhibited for a well width of $d = 5$ nm (normal regime) compared to one with $d = 7$ nm (topological regime). We have pinpointed the origin of this finding as the sizable interband exchange correction whose sign differs in the topological and normal regimes. Thus a measurement of the quantum capacitance of HgTe quantum wells, e.g., using HgTe double-quantum-well configurations [48], provides a useful way to determine the topological state of this system.

The enhancement and eventual sign change of the compressibility found in the low-density limit of the nontopological phase are analogous to the behavior exhibited by ordinary 2D electron systems with parabolic dispersion [3–9]. In contrast, the compressibility of the 2D electron system in the topological phase is strongly suppressed by Coulomb interactions. Additional contributions to the compressibility arising from image charges [16,17] and disorder [49] can be straightforwardly included to facilitate the description of real samples.

[1] T. P. Smith, B. B. Goldberg, P. J. Stiles, and M. Heiblum, Phys. Rev. B **32**, 2696 (1985).
[2] S. Luryi, Appl. Phys. Lett. **52**, 501 (1988).
[3] S. V. Kravchenko, D. A. Rinberg, S. G. Semenchinsky, and V. M. Pudalov, Phys. Rev. B **42**, 3741 (1990).
[4] J. P. Eisenstein, L. N. Pfeiffer, and K. W. West, Phys. Rev. Lett. **68**, 674 (1992).
[5] J. P. Eisenstein, L. N. Pfeiffer, and K. W. West, Phys. Rev. B **50**, 1760 (1994).
[6] S. Shapira, U. Sivan, P. M. Solomon, E. Buchstab, M. Tischler, and G. Ben Yoseph, Phys. Rev. Lett. **77**, 3181 (1996).
[7] I. S. Millard, N. K. Patel, C. L. Foden, E. H. Linfield, M. Y. Simmons, D. A. Ritchie, and M. Pepper, Phys. Rev. B **55**, 6715 (1997).
[8] S. C. Dultz and H. W. Jiang, Phys. Rev. Lett. **84**, 4689 (2000).
[9] G. Allison, E. A. Galaktionov, A. K. Savchenko, S. S. Safonov, M. M. Fogler, M. Y. Simmons, and D. A. Ritchie, Phys. Rev. Lett. **96**, 216407 (2006).
[10] J. Martin, N. Akerman, G. Ulbricht, T. Lohmann, J. H. Smet, K. von Klitzing, and A. Yacoby, Nat. Phys. **4**, 144 (2008).
[11] E. A. Henriksen and J. P. Eisenstein, Phys. Rev. B **82**, 041412 (2010).
[12] L. Li, C. Richter, S. Paetel, T. Kopp, J. Mannhart, and R. C. Ashoori, Science **332**, 825 (2011).
[13] A. F. Young, C. R. Dean, I. Meric, S. Sorgenfrei, H. Ren, K. Watanabe, T. Taniguchi, J. Hone, K. L. Shepard, and P. Kim, Phys. Rev. B **85**, 235458 (2012).
[14] D. A. Kozlov, D. Bauer, J. Ziegler, R. Fischer, M. L. Savchenko, Z. D. Kvon, N. N. Mikhailov, S. A. Dvoretsky, and D. Weiss, Phys. Rev. Lett. **116**, 166802 (2016).
[15] G. Giuliani and G. Vignale, *Quantum Theory of the Electron Liquid* (Cambridge University Press, Cambridge, UK, 2005); See also the early work by M. S. Bello, E. I. Levin, B. I. Shklovskii, and A. L. Efros, Zh. Eksp. Teor. Fiz. **80**, 1596 (1981) [Sov. Phys. JETP **53**, 822 (1981)].
[16] B. Skinner and B. I. Shklovskii, Phys. Rev. B **82**, 155111 (2010).
[17] B. Skinner and M. M. Fogler, Phys. Rev. B **82**, 201306 (2010).
[18] Q. Li, E. H. Hwang, and S. Das Sarma, Phys. Rev. B **84**, 235407 (2011).
[19] E. H. Hwang, B. Yu-Kuang Hu, and S. Das Sarma, Phys. Rev. Lett. **99**, 226801 (2007).
[20] S. V. Kusminskiy, J. Nilsson, D. K. Campbell, and A. H. Castro Neto, Phys. Rev. Lett. **100**, 106805 (2008).
[21] G. Borghi, M. Polini, R. Asgari, and A. H. MacDonald, Phys. Rev. B **82**, 155403 (2010).
[22] D. S. L. Abergel, E. H. Hwang, and S. Das Sarma, Phys. Rev. B **83**, 085429 (2011).
[23] B. Tanatar and D. M. Ceperley, Phys. Rev. B **39**, 5005 (1989).
[24] M. König, S. Wiedmann, C. Brüne, A. Roth, H. Buhmann, L. W. Molenkamp, X. Qi, and S. Zhang, Science **318**, 766 (2007).
[25] A. Roth, C. Brüne, H. Buhmann, L. W. Molenkamp, J. Maciejko, X. Qi, and S. Zhang, Science **325**, 294 (2009).

[26] C. Brüne, A. Roth, H. Buhmann, E. M. Hankiewicz, L. W. Molenkamp, J. Maciejko, X.-L. Qi, and S.-C. Zhang, Nat. Phys. **8**, 485 (2012).

[27] S. Hart, H. Ren, M. Kosowsky, G. Ben-Shach, P. Leubner, C. Brüne, H. Buhmann, L. W. Molenkamp, B. I. Halperin, and A. Yacoby, arXiv:1509.02940.

[28] B. A. Bernevig, T. L. Hughes, and S. Zhang, Science **314**, 1757 (2006).

[29] M. König, H. Buhmann, L. W. Molenkamp, T. Hughes, C.-X. Liu, X.-L. Qi, and S.-C. Zhang, J. Phys. Soc. Jpn. **77**, 031007 (2008).

[30] R. Winkler, L. Wang, Y. Lin, and C. Chu, Solid State Commun. **152**, 2096 (2012).

[31] S. A. Tarasenko, M. V. Durnev, M. O. Nestoklon, E. L. Ivchenko, J.-W. Luo, and A. Zunger, Phys. Rev. B **91**, 081302 (2015).

[32] X. Qi and S. Zhang, Rev. Mod. Phys. **83**, 1057 (2011).

[33] C. Liu, T. L. Hughes, X.-L. Qi, K. Wang, and S.-C. Zhang, Phys. Rev. Lett. **100**, 236601 (2008).

[34] I. Knez, R.-R. Du, and G. Sullivan, Phys. Rev. Lett. **107**, 136603 (2011).

[35] M. Z. Hasan and J. E. Moore, Annu. Rev. Condens. Matter Phys. **2**, 55 (2011).

[36] S. Juergens, P. Michetti, and B. Trauzettel, Phys. Rev. Lett. **112**, 076804 (2014).

[37] S. Juergens, P. Michetti, and B. Trauzettel, Phys. Rev. B **90**, 115425 (2014).

[38] T. Kernreiter, M. Governale, U. Zülicke, and E. M. Hankiewicz, Phys. Rev. X **6**, 021010 (2016).

[39] M. Mühlbauer, A. Budewitz, B. Büttner, G. Tkachov, E. M. Hankiewicz, C. Brüne, H. Buhmann, and L. W. Molenkamp, Phys. Rev. Lett. **112**, 146803 (2014).

[40] R. Winkler, *Spin-Orbit Coupling Effects in Two-Dimensional Electron and Hole Systems* (Springer, Berlin, 2003).

[41] D. A. Broido and L. J. Sham, Phys. Rev. B **31**, 888 (1985).

[42] S.-R. E. Yang, D. A. Broido, and L. J. Sham, Phys. Rev. B **32**, 6630 (1985).

[43] The right-hand side of Eq. (9) can be expressed as $\pi\hbar^2/m_*$, where m_* is the effective band mass of 2D electrons obtained from the small-k expansion of the dispersion (4).

[44] The intraband Fock contribution to $D_{\rm T}^{-1}$ diverges $\propto k_{\rm F}^{-1}$ in the low-density limit, as the Fock contribution for an ordinary 2D electron gas [17]. In real samples, this divergence is cut off by image-charge effects [16,17].

[45] The BHZ parameters A and B are generally only weakly dependent on the HgTe quantum-well width d (see Table I) and, for this calculation, we use the A and B values for $d = 7$ nm. The mass parameter M, on the other hand, depends sensitively on d, and we extract its functional dependence from the band-edge energies of the conduction and valence bands, which are obtained by appropriate matching conditions derived from the relevant confined-electron problem (see the Supplemental Material of Ref. [28]). Note that the BHZ parameter D does not enter the exchange corrections to $D_{\rm T}^{-1}$.

[46] See Supplemental Material at http://link.aps.org/supplemental/10.1103/PhysRevB.93.241304 for an illustration of a divergence in the interband Fock contribution to $D_{\rm T}^{-1}$ for $k_{\rm F} \to 0$, and for more details about the relative unimportance of spin-orbit-coupling effects.

[47] D. G. Rothe, R. W. Reinthaler, C.-X. Liu, L. W. Molenkamp, S.-C. Zhang, and E. M. Hankiewicz, New J. Phys. **12**, 065012 (2010).

[48] M. V. Yakunin, A. V. Suslov, M. R. Popov, E. G. Novik, S. A. Dvoretsky, and N. N. Mikhailov, Phys. Rev. B **93**, 085308 (2016).

[49] M. M. Fogler, Phys. Rev. B **69**, 121409 (2004).